Lawrence Berkeley National Laboratory

Title

Templated encapsulation of platinum-based catalysts promotes high-temperature stability to 1,100 °C

Permalink

https://escholarship.org/uc/item/61p8w7ft

Journal

Nature Materials, 21(11)

ISSN

1476-1122

Authors

Aitbekova, Aisulu
Zhou, Chengshuang
Stone, Michael L
et al.

Publication Date

2022-11-01

DOI

10.1038/s41563-022-01376-1

Copyright Information

Peer reviewed

Templated Encapsulation of Pt-based Catalysts Promotes High-Temperature Stability to 1,100 °C

Aisulu Aitbekova[1], Chengshuang Zhou[1], Michael L. Stone[1], Juan Salvador Lezama-Pacheco[2], An-Chih Yang[1], Adam S. Hoffman[3], Emmett D. Goodman[1], Philipp Huber[4], Jonathan F. Stebbins[6], Karen C. Bustillo[5], Peter Ercius[5], Jim Ciston[5], Simon R. Bare[3], Philipp N. Plessow[4], Matteo Cargnello[1,*]

[1]*Department of Chemical Engineering and SUNCAT Center for Interface Science and Catalysis, Stanford University, Stanford, CA 94305, USA*
[2]*Department of Earth System Science, Stanford University, Stanford, CA 94305, USA*
[3]*Stanford Synchrotron Radiation Lightsource, SLAC National Accelerator Laboratory, Menlo Park, California 94025, United States*
[4]*Institute of Catalysis Research and Technology, Karlsruhe Institute of Technology, Karlsruhe, 76131, Germany*
[5]*National Center for Electron Microscopy, Molecular Foundry, Lawrence Berkeley National Laboratory, Berkeley, CA 94720, USA*
[6]*Department of Geological Sciences, Stanford University, Stanford, CA 94305, USA*

[*]Corresponding author: mcargnello@stanford.edu (M.C.)

Sintering simulations in absence of diffusion limitations
The theory behind the mean-field model for the simulation of $PtO_2(g)$ in absence of diffusion limitations is the same as described in the literature.[1] Neglecting diffusion limitations, immediate transport of $PtO_2(g)$ through the gas phase leads to a constant $PtO_2(g)$ pressure p_b in the entire system. The influx of $PtO_2(g)$ onto a given particle follows the ideal gas law based on pressure p_b, mass m, temperature T, and surface area of the particle A(r):

$$J_{in} = \frac{S}{\sqrt{2\pi mkT}} \cdot A(r) \cdot p_b \qquad (S1)$$

The total flux according to the mean-field model is given by:

$$J_{tot} = \frac{S}{\sqrt{2\pi mkT}} \cdot A(r) \cdot [p_b - p_{eq}(r)] \qquad (S2)$$

Importantly, $p_{eq}(r)$ depends only on the thermodynamic stability of $PtO_2(g)$ relative to the chemical potential of the particle and it is not an observable pressure. In the mean field model, p_b is then determined from the requirement of mass-conservation, which means that the sum of the fluxes J_{tot} of all particles is zero.

Sintering simulations and diffusion limitations
Above, we considered the limiting case that fast diffusion will immediately equilibrate the gas phase containing all particles. We now study the opposite case, where diffusion through the encapsulating material is slow. In the limiting case of extremely slow diffusion, an equilibrium between the particles and $PtO_2(g)$ within the encapsulating material will be established with the local pressure $p_{eq}(r)$, which is different for each particle. Outside of the particle, fast diffusion is assumed to again establish a constant background pressure p_b. Diffusion through the encapsulating material with constant diffusion coefficient D and surface area A is described by Fick's first law:

$$J_{tot} = -AD\nabla c \qquad (S3)$$

Here, ∇c is the concentration gradient of the diffusing species, $PtO_2(g)$. For an encapsulating wall of constant thickness d, we obtain a constant concentration gradient:

$$J_{tot} = -AD\left(\frac{c_{eq} - c_b}{d}\right) \qquad (S4)$$

Expressing the concentrations in terms of pressures using the ideal gas law, we obtain:

$$J_{tot} = \frac{D}{dkT} A(p_b - p_{eq}). \qquad (S5)$$

Equation S5 has the same functional form as equation S2. If we assume that the area of the encapsulating material, through which $PtO_2(g)$ diffuses, is proportional to that of the particle, then identical results are obtained with both types of simulations, if the pre-factors are equal:

$$\frac{S}{\sqrt{2\pi mkT}} \cdot A = \frac{D}{dkT} A \qquad (S6)$$

Consequently, the results of a sintering simulation with strong diffusion limitations and the parameters (D, d, T, A) give exactly the same results as simulations without diffusion limitations, if an appropriate value of $S=S_{eff}$ is chosen. Here, we use S_{eff} rather than S to emphasize that it effectively captures diffusion limitations and is not the sticking coefficient of a clean surface.

Effect of diffusion limitations on catalysis
Assuming that the diffusion coefficient of $PtO_2(g)$ and $O_2(g)$ is the same, the effect of the diffusion limitations, as expressed through a given S_{eff} can be estimated. Under steady-state conditions, the rate of O_2-consumption per particle (TOF) equals the flux of $O_2(g)$ through the encapsulating material.

$$TOF = J_{tot} \qquad (S7)$$

Using Eq. S5, we can determine the pressure drop Δp between the O_2-pressure outside and inside the encapsulation that is caused by the diffusion limitations:

$$\Delta p = TOF / \left(\frac{D}{dkT} A \right) \quad (S8)$$

We will now study a worst-case scenario, where Δp becomes largest. The highest measured consumption rate of $O_2(g)$ was determined as 695 molecules per second and nanoparticle at 202 °C. The smallest estimate of the diffusion limitations follows from Fig. 4b, for S_{eff} = 0.001 at 800°C. In order to account for the fact that diffusion is expected to be slower at lower temperatures, we assume a temperature dependence of D~$T^{3/2}$. Using Eq. S8 and the surface area of a spherical particle with d=3.8 nm, we obtain a pressure drop of $\Delta p = 4.3 * 10^{-5} bar$. For an oxygen pressure of 0.03 bar of $O_2(g)$, this means that the O_2-pressure is reduced by about 0.1%. The analogous calculation can be performed for propene. Since combustion per formula unit C_3H_6 requires 9/2 O_2 molecules, the pressure drop is reduced by a factor of 2/9 to $0.96 * 10^{-5} bar$. Relative to the partial pressure of propene, $1.5 * 10^{-3} bar$, this is again a negligible pressure drop of 0.6 %.

The example above shows that the diffusion limitations assumed to be present for sintering via $PtO_2(g)$ have no significant effect on catalysis. The reason for this is that the induced pressure gradient for O_2 is very small compared to the pressure of O_2. For sintering, however, the situation is different, since the pressure of $PtO_2(g)$ is typically on the order of 10^{-9} bar. Therefore, much smaller pressure drops will already be significant for sintering.

To study the effect of longer sintering time, a sintering protocol under alternating reducing/oxidizing conditions over 50 h was also considered (Table S5). Here, only a third of the 50 h is under oxidizing conditions, while the remaining time is spent under reducing conditions. Since the partial pressure of $PtO_2(g)$ will be negligible under reducing conditions, we modeled this situation by only considering a sintering time of is 50/3 h ≈ 16.67 h under oxidizing conditions (900 °C and 1.5% O_2). All other parameters were kept the same.
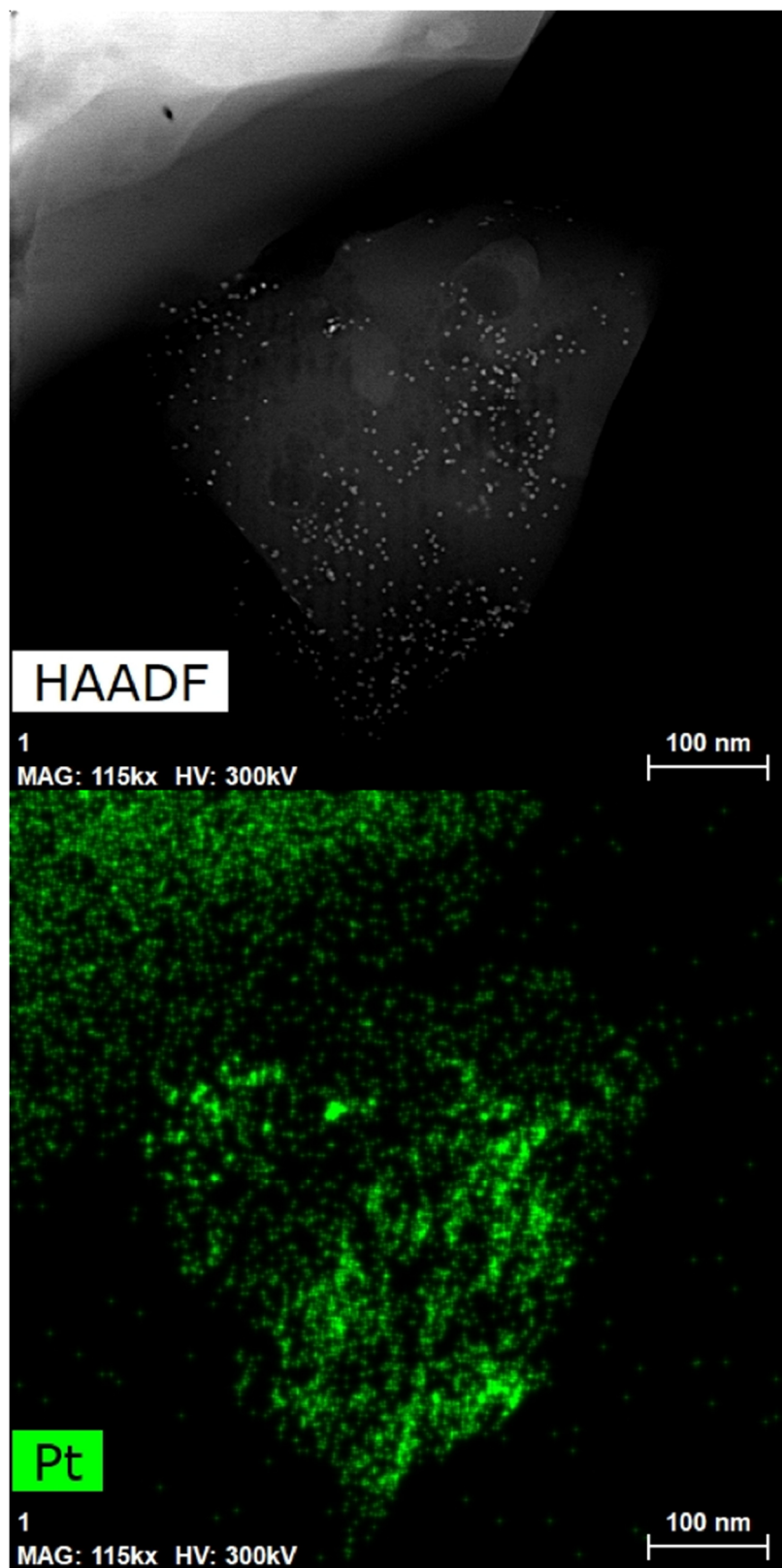
Figure S1. HAADF-STEM image and corresponding Pt-L edge EDS map of as-synthesized Pt@Al$_2$O$_3$.

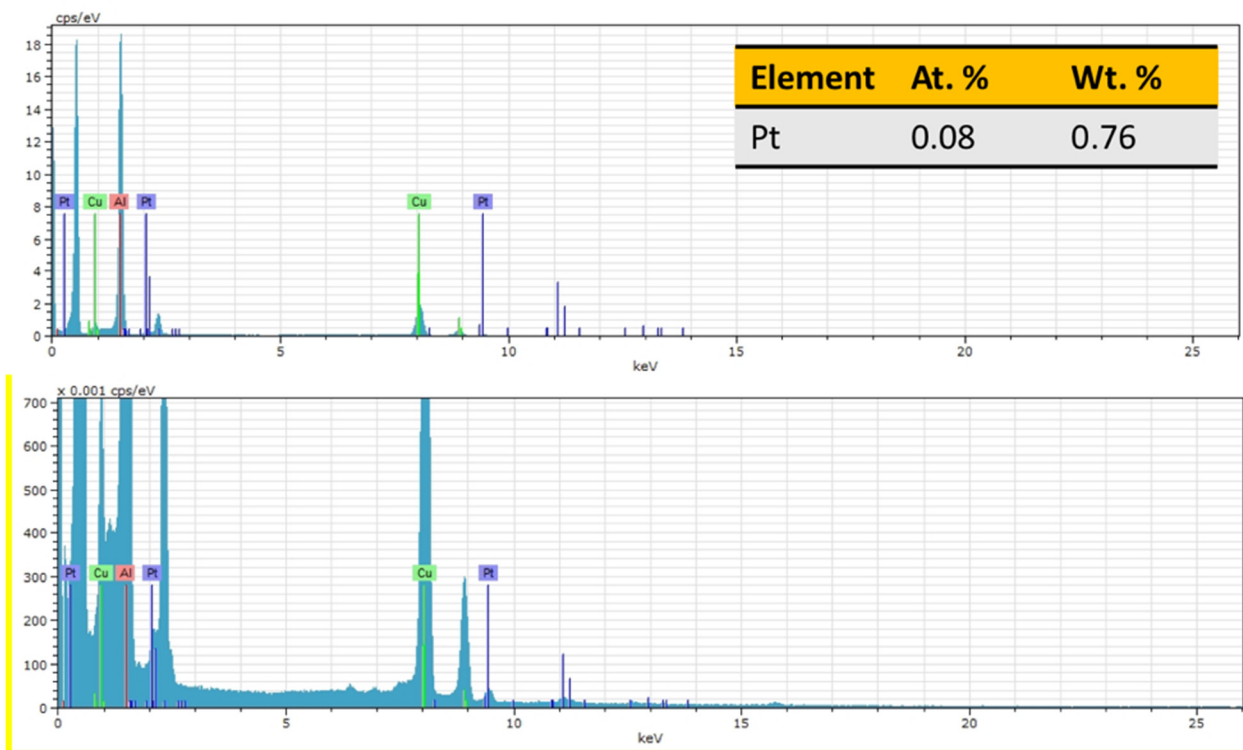| Element	At. %	Wt. %
Pt	0.08	0.76

Figure S2. EDS spectrum corresponding to the EDS map in Figure S1 showing Pt-L edge. Fe, Co, Cu, Zr, and Sn normal signal from the TEM column/holder. Pt atomic and weight percent concentrations measured from EDS: 0.08 at. % or 0.76 wt. %.
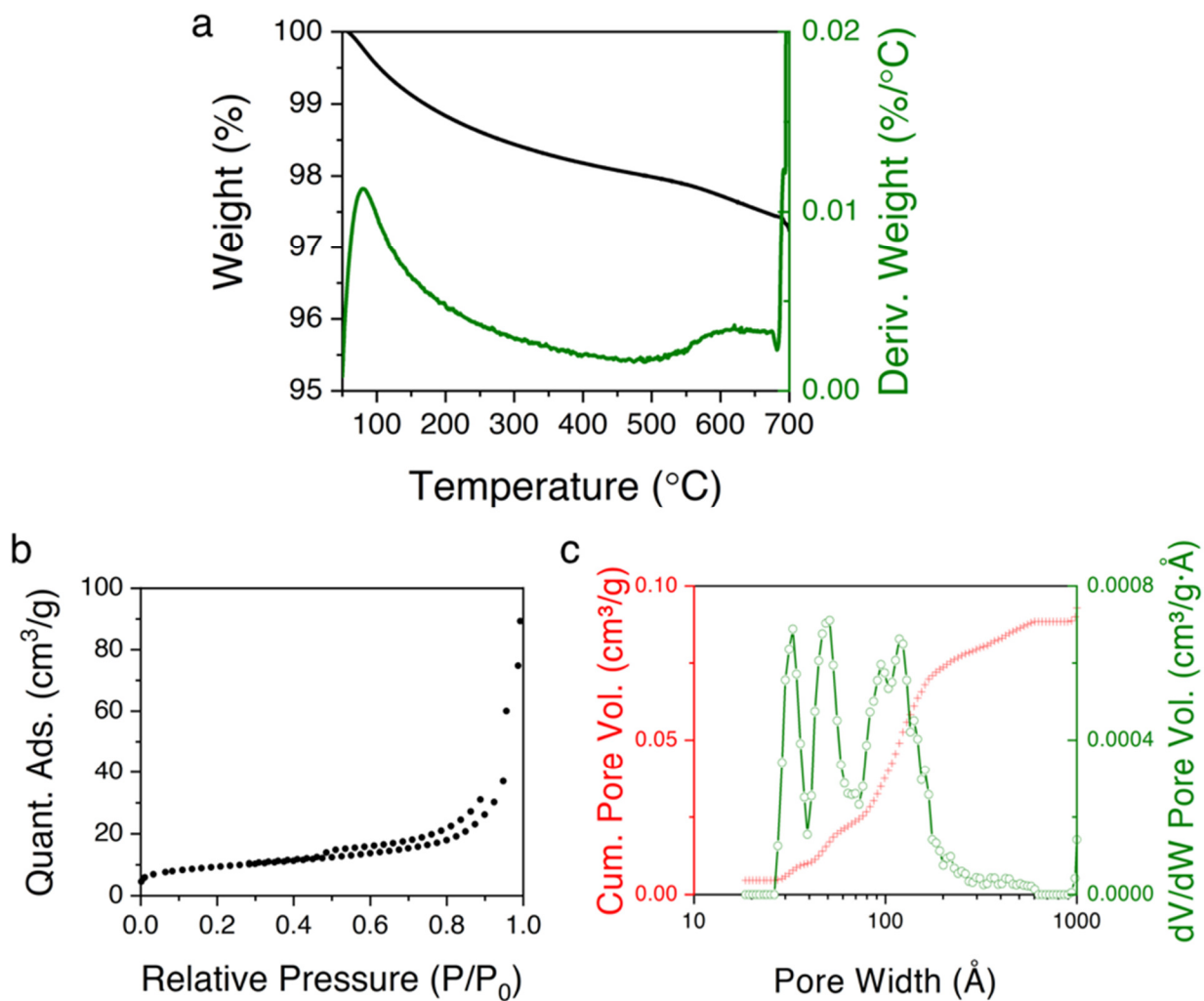
Figure S3. a-c) Characterization of Pt@Al$_2$O$_3$: a) TGA upon heating the sample in air to 700°C; b) N$_2$ physisorption isotherm; c) pore size distribution.
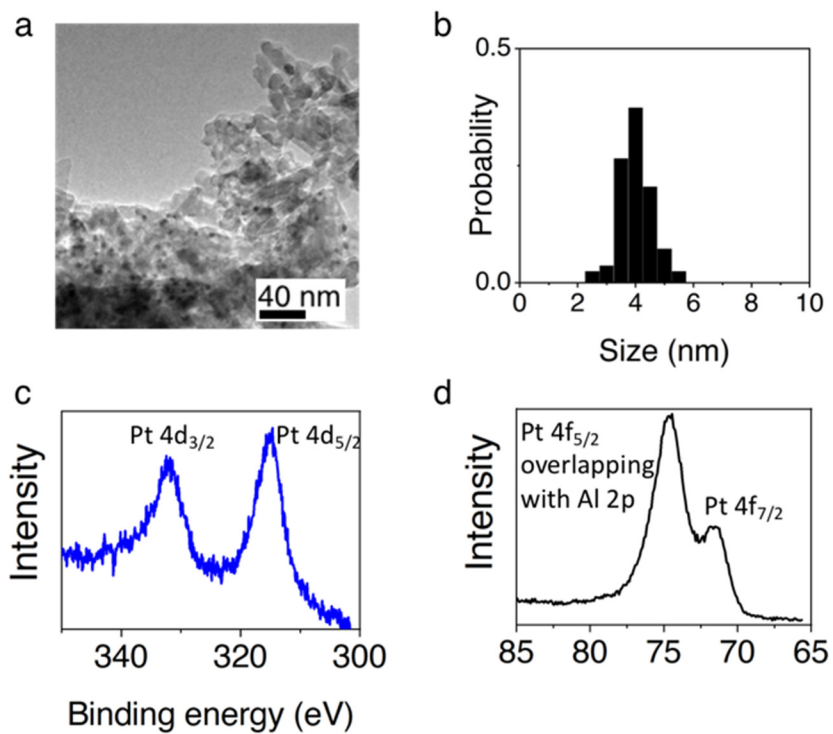
Figure S4. Characterization of Pt/Al$_2$O$_3$: a) Transmission electron microscopy image; b) NP size distribution; c-d) XPS of c) Pt 4d$_{3/2}$ (332.2 eV) and Pt 4d$_{5/2}$ (315.2 eV); d) Al 2p (74.7 eV) and Pt 4f$_{5/2}$ (71.5 eV) overlapping signals.
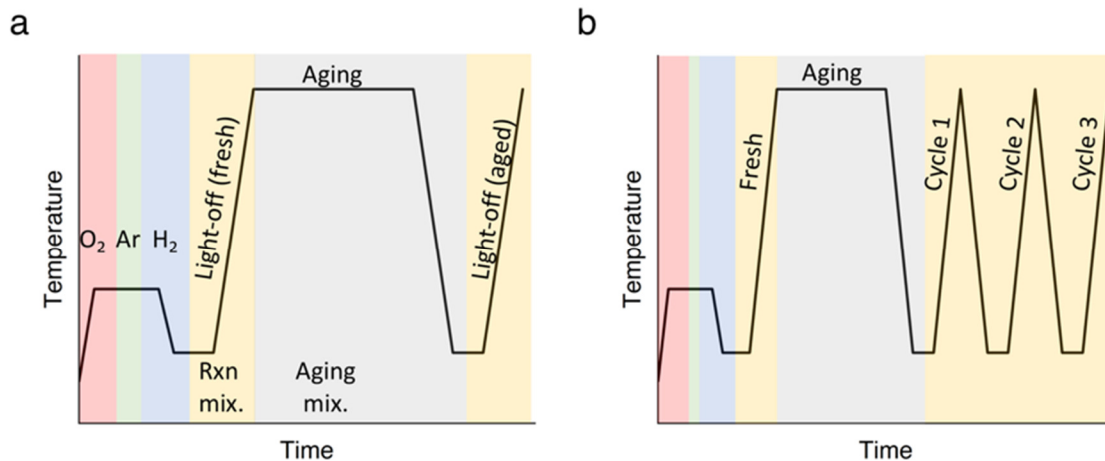
Figure S5. a) Temperature profile and catalyst environment for one aging cycle; b) Temperature profile and catalyst environment for three consecutive cycles.
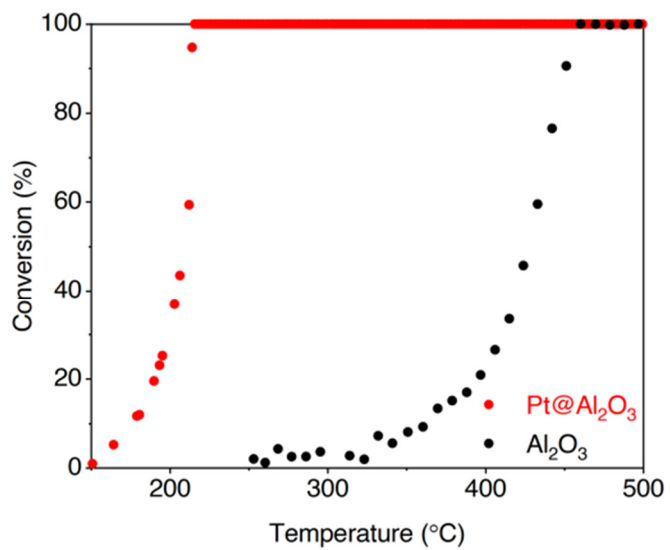
Figure S6. Light-off curves of fresh Pt@Al$_2$O$_3$ and metal-free Al$_2$O$_3$ support. Reaction mixture: 0.15 vol.% C$_3$H$_6$, 3 vol.% O$_2$, and 5 vol.% steam (balance Ar).
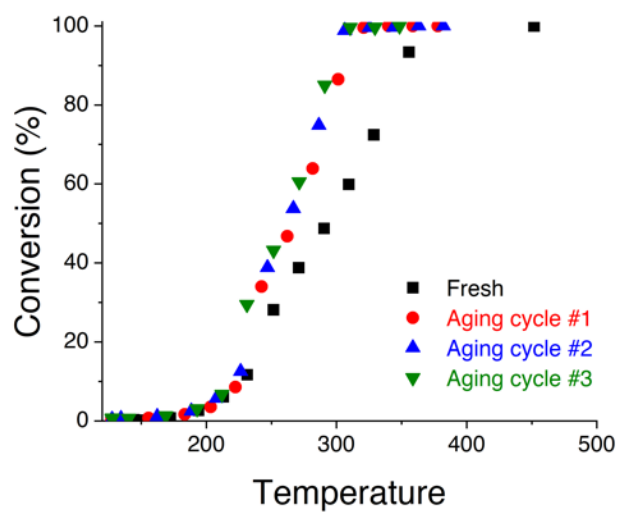
Figure S7. Propene combustion activity for as-prepared Pt@Al$_2$O$_3$ and the aged catalyst after consecutive three cycles (aging performed at 800 °C for 2 h in the reaction mixture). 30 mg of the catalyst was mixed with 160 mg of SiC diluent. Catalyst pretreatment: 300 °C, 30 min 5 vol.% O$_2$ (40 mL/min), 10 min Ar (40 mL/min), 30 min 5 vol.% H$_2$ (40 mL/min). Reaction mixture: 0.15 vol.% C$_3$H$_6$, 3 vol.% O$_2$, 5 vol.% H$_2$O, balance Ar (50 mL/min total flow rate).
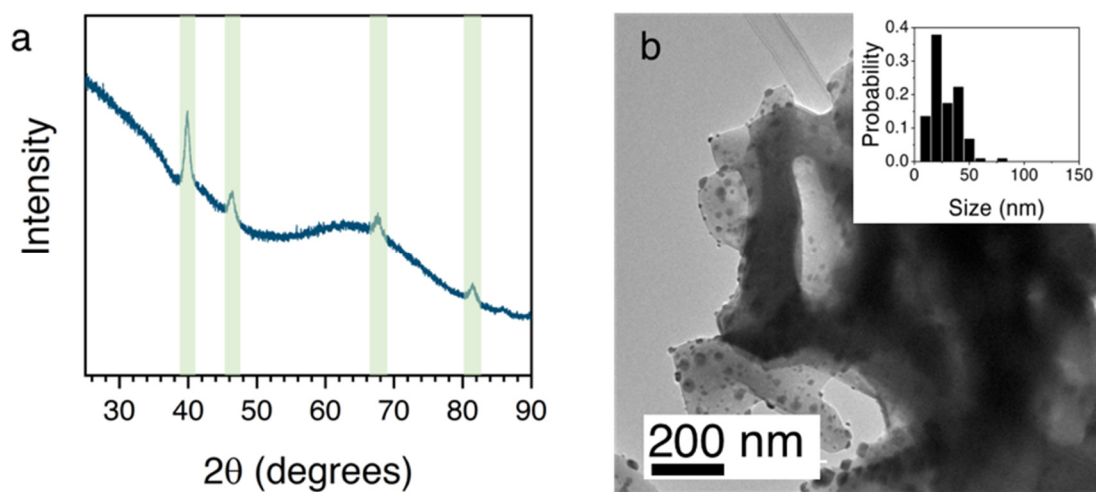
Figure S8. Characterization of Pt/Al$_2$O$_3$ calcined at 600 °C. a) XRD: highlighted peaks are due to metallic Pt; b) TEM: upon calcination the average Pt NP size increases from 3.8 nm to 23.3 nm.
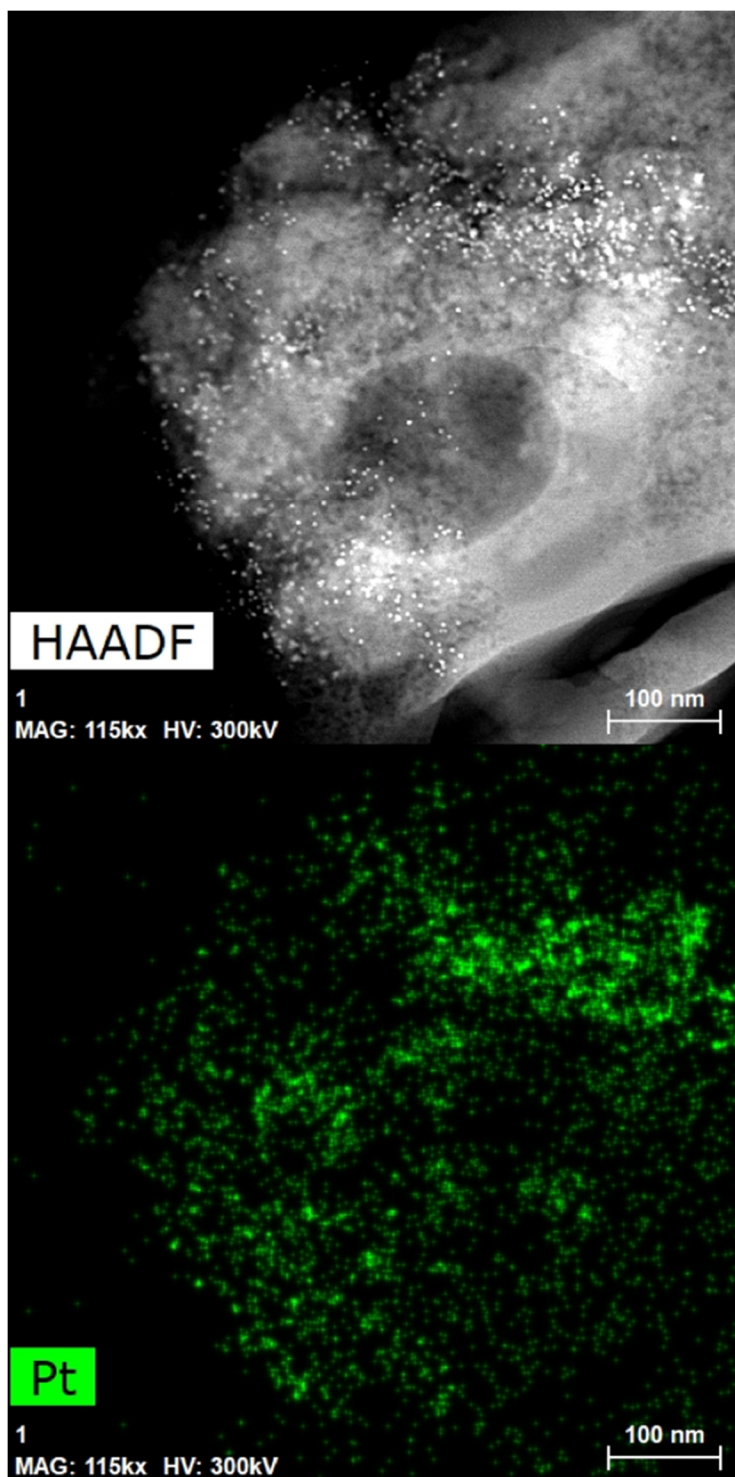
Figure S9. HAADF-STEM image and corresponding Pt-L edge EDS map of aged Pt@Al$_2$O$_3$-800.
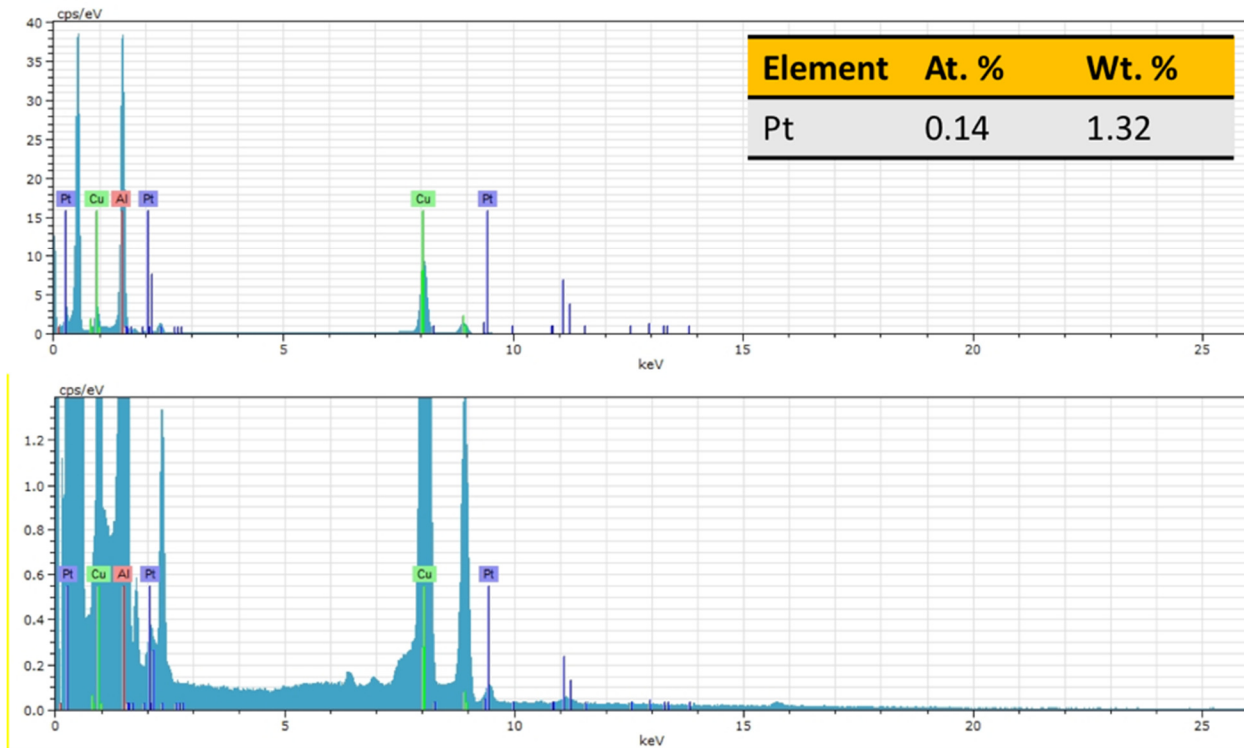
Element	At. %	Wt. %
Pt	0.14	1.32

Figure S10. EDS spectrum corresponding to the EDS map in Figure S9 showing Pt-L edge. Fe, Co, Cu, Zr, and Sn normal signal from the TEM column/holder. Pt atomic and weight percent concentrations measured from EDS: 0.14 at. % or 1.32 wt. %.
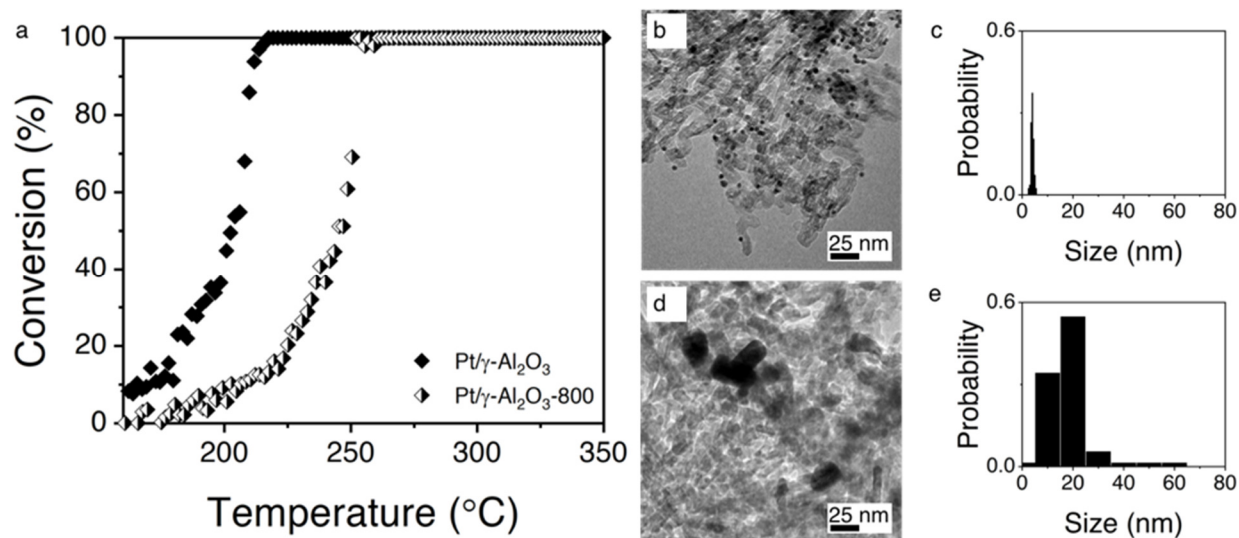
Figure S11. a) Light-off curve measurements of fresh and aged Pt/γ-Al$_2$O$_3$. Reaction conditions: 0.15 vol. % C$_3$H$_6$, 3 vol. % O$_2$, and 5 vol. % steam, balance Ar (40 ml/min total flow). Aging performed in the reaction mixture at 800 °C for 2 h; b-e) Representative TEM images and particle size distributions of the fresh (b-c) and aged catalysts (d-e).
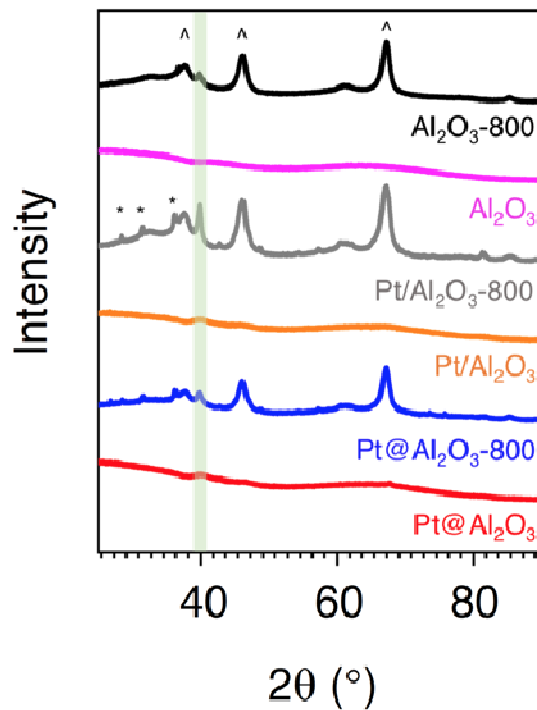
Figure S12. XRD patterns for the samples and the bare support. ^ and * represent diffractions peaks due to γ-Al_2O_3 and quartz diluent, respectively. Highlighted region at 40° indicates overlapping γ-Al_2O_3 and Pt(111) diffraction peaks.
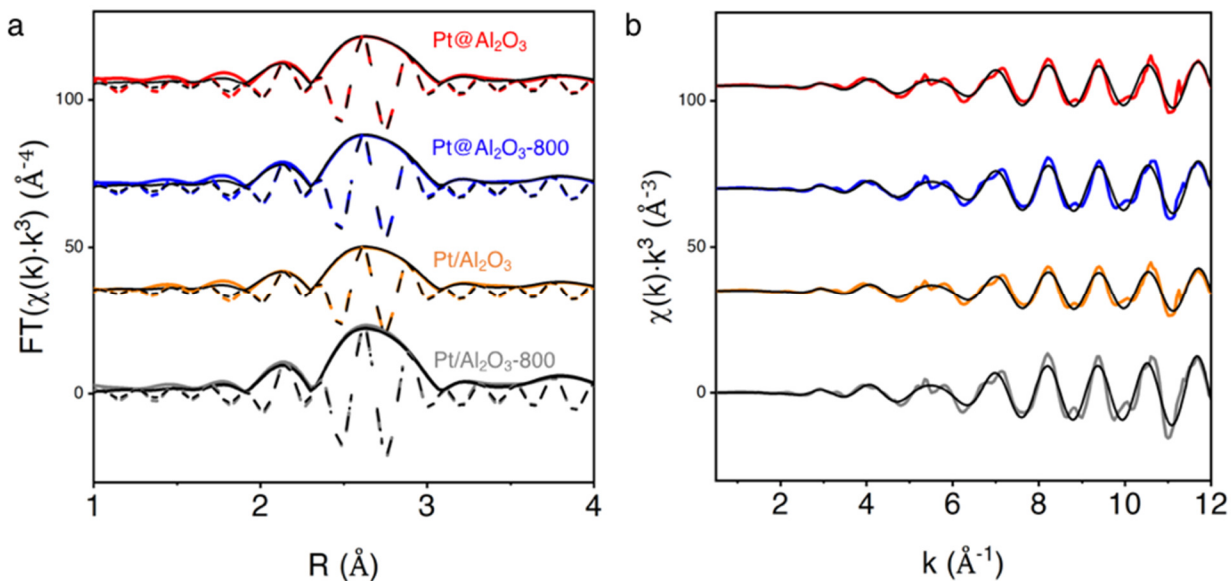
Figure S13. a) Magnitude and imaginary part of the Fourier Transform and b) EXAFS of the Pt L$_3$-edge data and best-fits characterizing the encapsulated and supported Pt catalysts before and after aging at 800°C. Black lines indicate the fits.
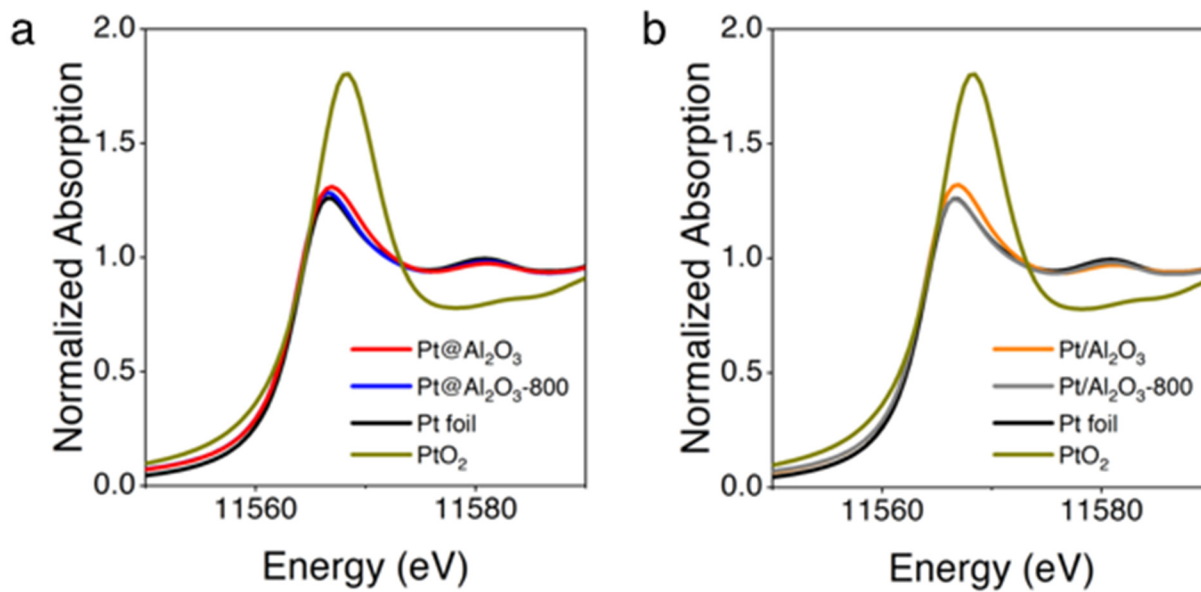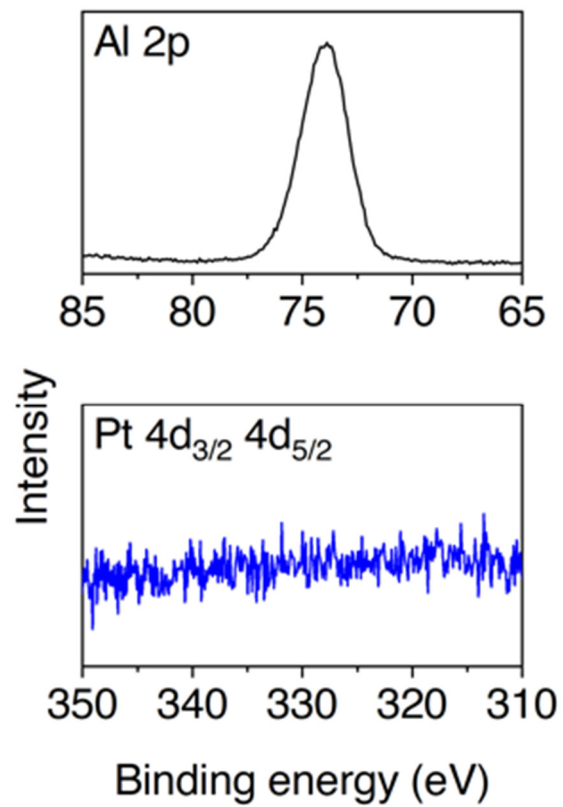
Figure S14. Pt L_3-edge XANES: a) Pt@Al_2O_3; b) Pt/Al_2O_3.

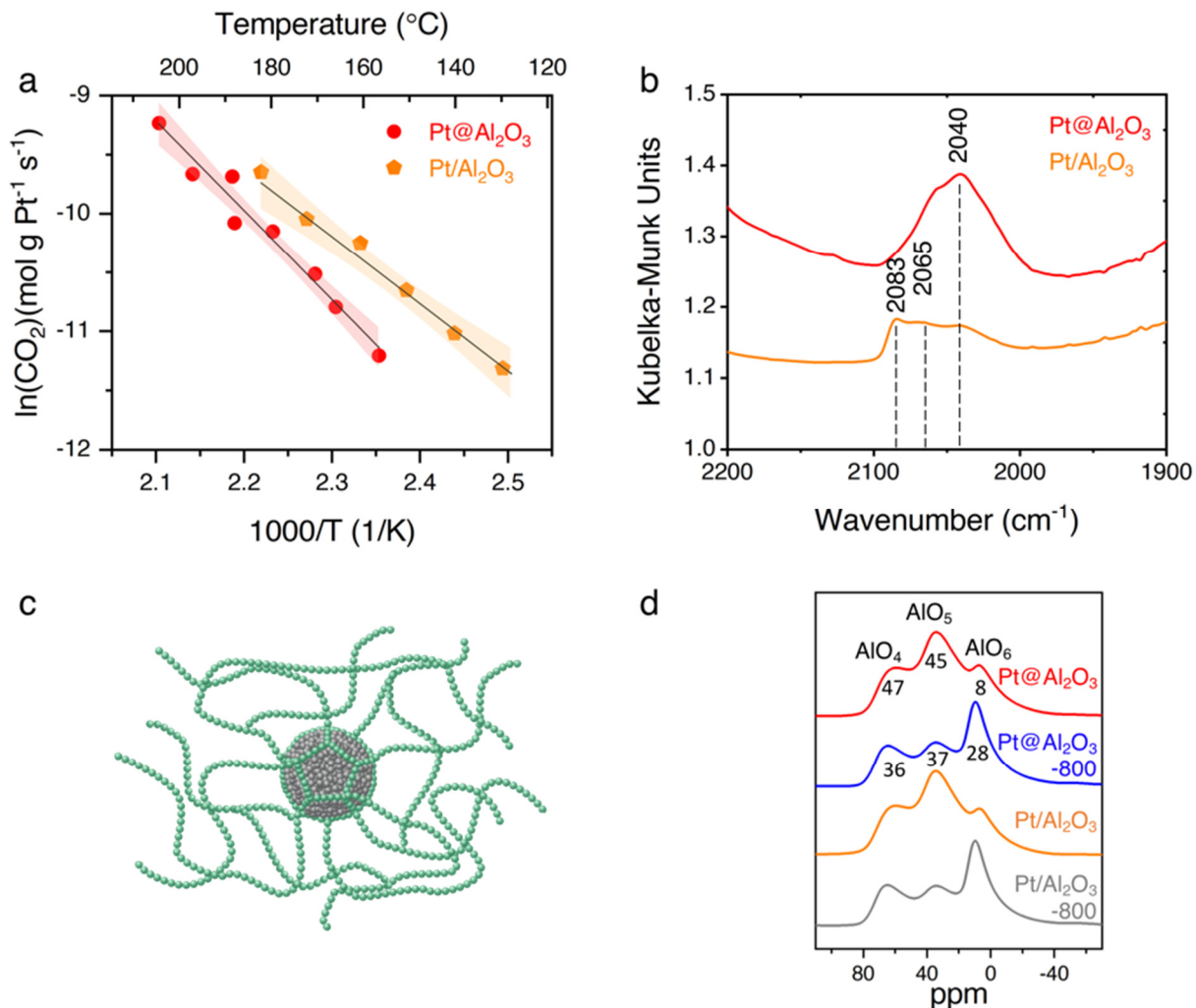**Figure S15.** XPS characterization of Pt@Al$_2$O$_3$-800.

Figure S16. a) Arrhenius plots with 95% confidence intervals of Pt@Al_2O_3 and Pt/Al_2O_3 for propene combustion collected at conversions less than 5%. The data points are averages for three measurements; b) CO diffuse reflectance infrared spectroscopy; c) proposed model schematic of Pt@Al_2O_3; d) ^{27}Al MAS NMR spectra of fresh and aged Pt@Al_2O_3 and Pt/Al_2O_3. Peaks for four-, five-, and six-coordinated Al (AlO_4, AlO_5, AlO_6) are labeled, with approximate percentages of each shown below the spectra.
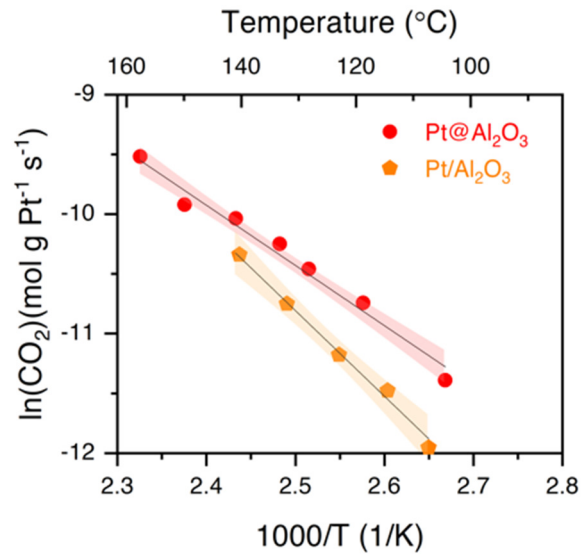
Figure S17. Arrhenius plots with 95% confidence intervals of Pt@Al$_2$O$_3$ and Pt/Al$_2$O$_3$ for CO oxidation collected at conversions less than 5%. The data points are averages for three measurements.

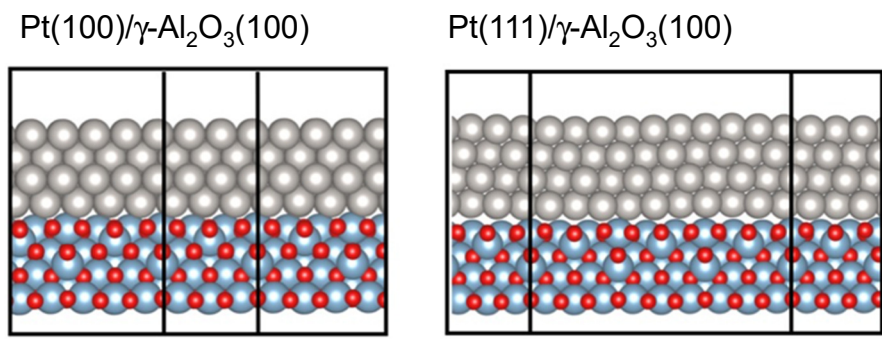Pt(100)/γ-Al$_2$O$_3$(100)   Pt(111)/γ-Al$_2$O$_3$(100)

Figure S18. Side-on views of the atomic models optimized for the interfaces of Pt(100) and Pt(111) with the γ-Al$_2$O$_3$(100) surface.
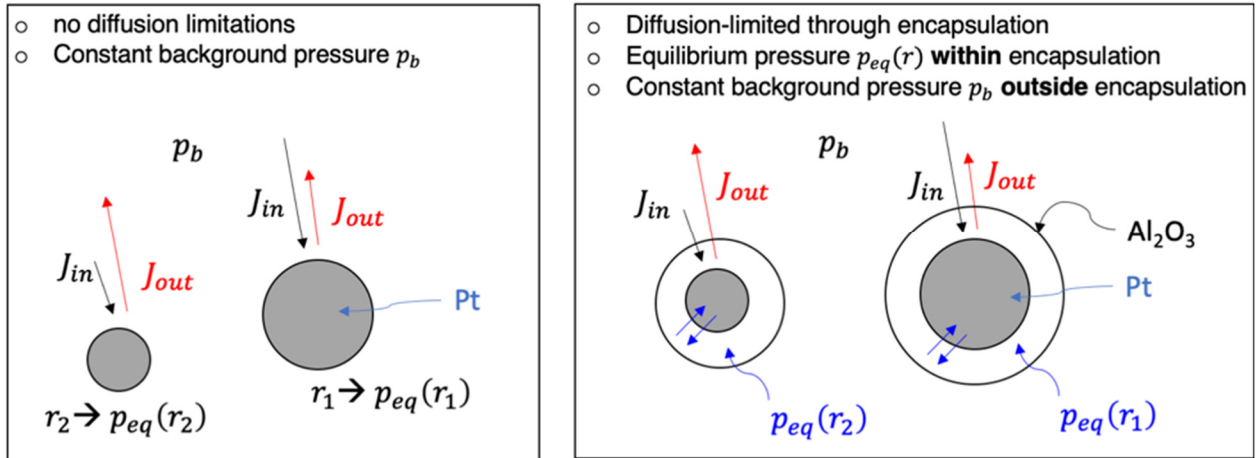
Figure S19. Illustration of sintering models and underlying assumptions: Left: No diffusion limitations lead to immediate equilibration within the gas phase und thus a constant background pressure p_b. Right: Significant diffusion limitations through the encapsulating material lead to local equilibration between particle and gas phase for each particle, so that locally the equilibrium pressure $p_{eq}(r)$ is established.

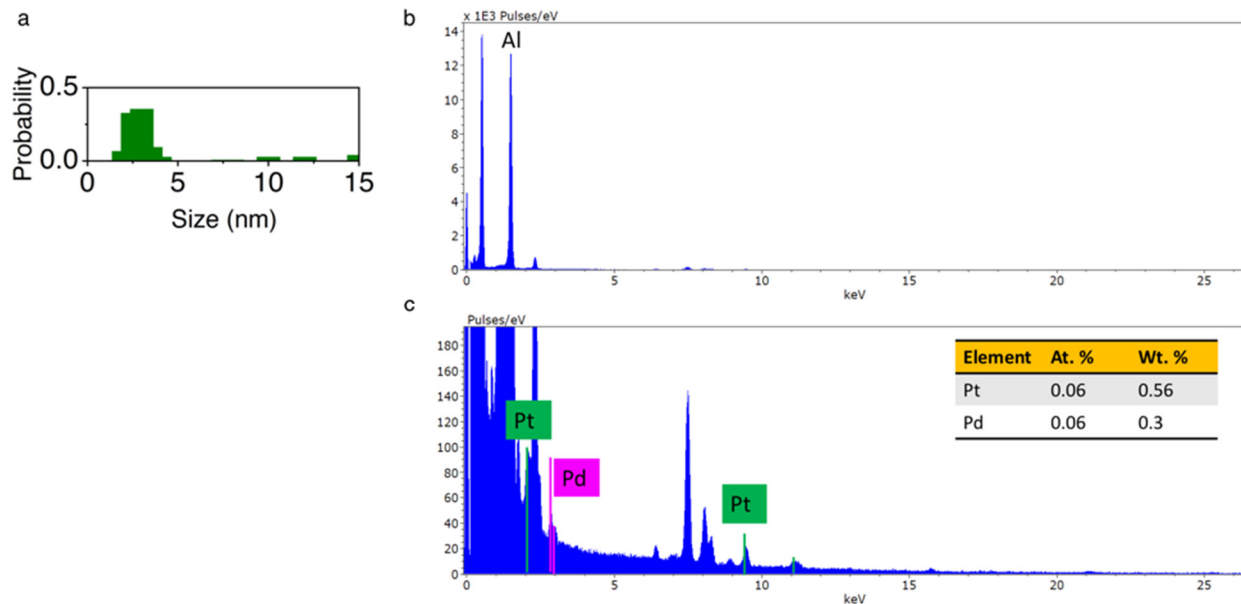**Figure S20.** Characterization of as-synthesized PdPt@Al$_2$O$_3$: a) Particle size distribution; b) EDS full spectrum; c) EDS spectrum <mark>corresponding to the EDS maps in Figures 4b-c</mark> showing Pd-K edge and Pt-L edge on Ni grid. Fe, Co, Cu, Zr, and Sn normal signal from the TEM column/holder. Pt and Pd atomic and weight percent concentrations measured from EDS: Pt 0.06 at.%, 0.56 wt.%; Pd 0.06 at.%, 0.3 wt.%.

Figure S21. HAADF-STEM image and corresponding EDS maps (Pd-K edge and Pt-L edge) of as-synthesized PdPt@Al$_2$O$_3$.

Element	At. %	Wt. %
Pt	0.02	0.20
Pd	0.03	0.13

Figure S22. EDS spectrum of as-synthesized PdPt@Al$_2$O$_3$ corresponding to the EDS maps in Figure S21 showing Pd-K edge and Pt-L edge on Ni grid. Fe, Co, Cu, Zr, and Sn normal signal from the TEM column/holder. Pt and Pd atomic and weight percent concentrations measured from EDS: Pt 0.02 at. %, 0.20 wt.%; Pd 0.03 at.%, 0.13 wt.%.
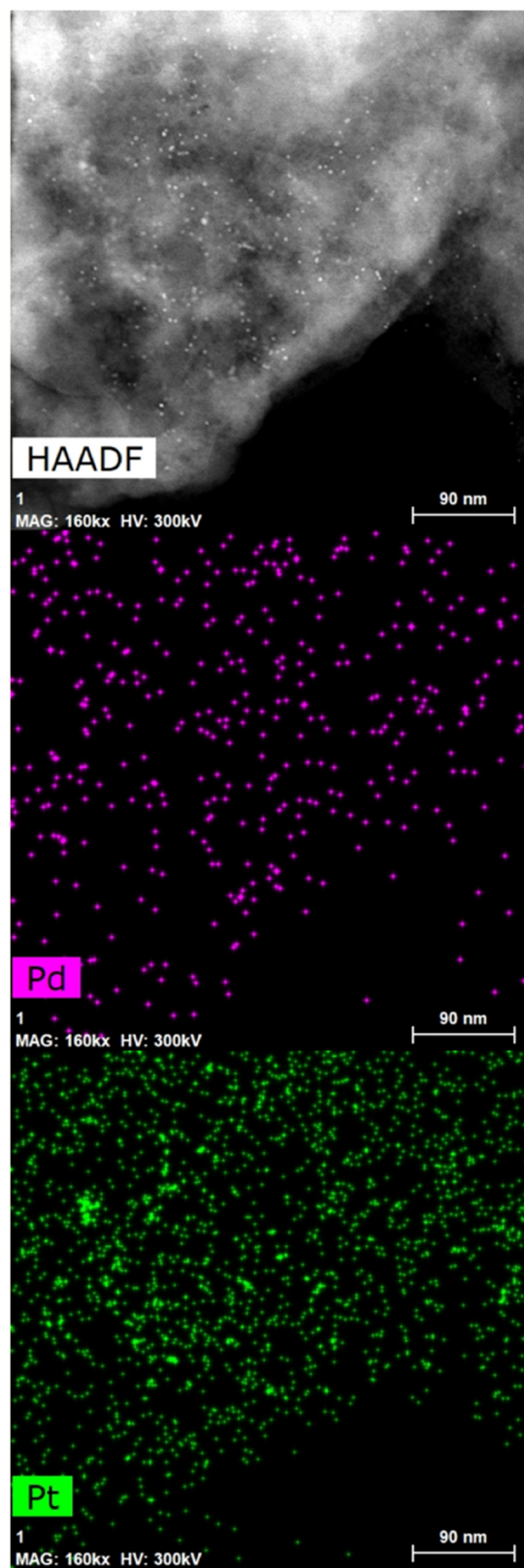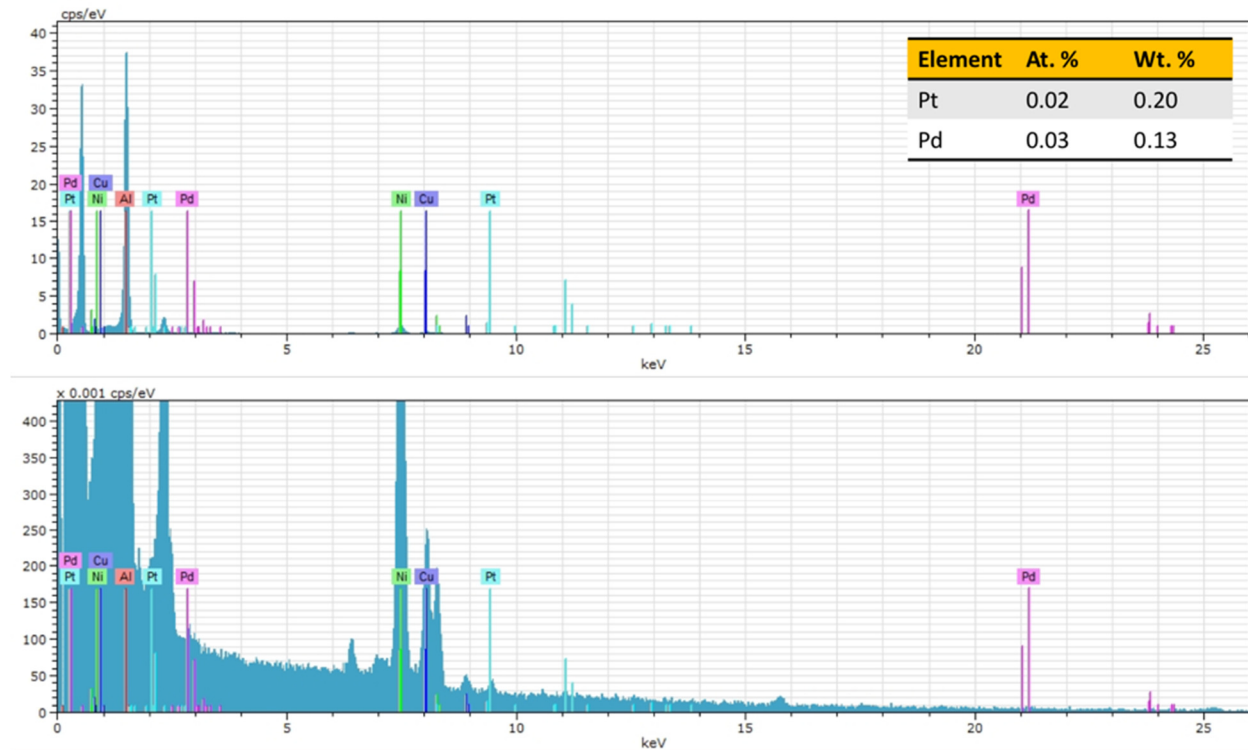
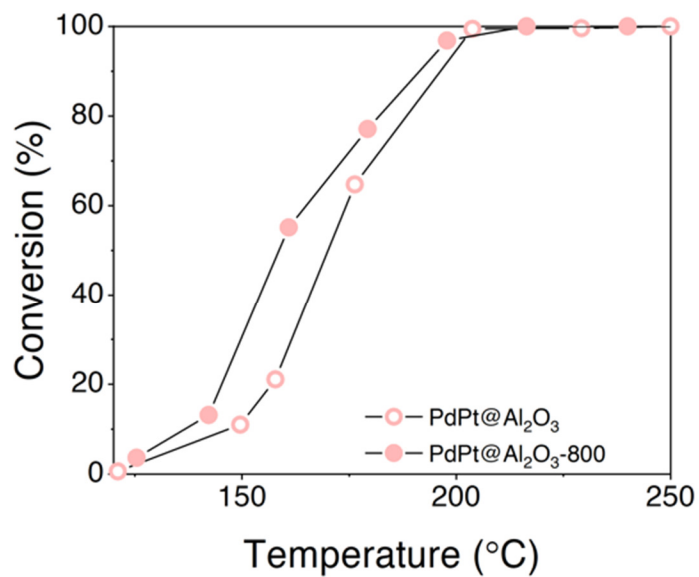**Figure S23.** a) Propene combustion activity for as-prepared and 800 °C aged PdPt@Al$_2$O$_3$. Aging conditions: 800 °C for 2 h in the reaction mixture consisting of 0.15 vol. % C$_3$H$_6$, 3 vol. % O$_2$, and 5 vol. % steam, balance Ar (40 ml/min total flow).
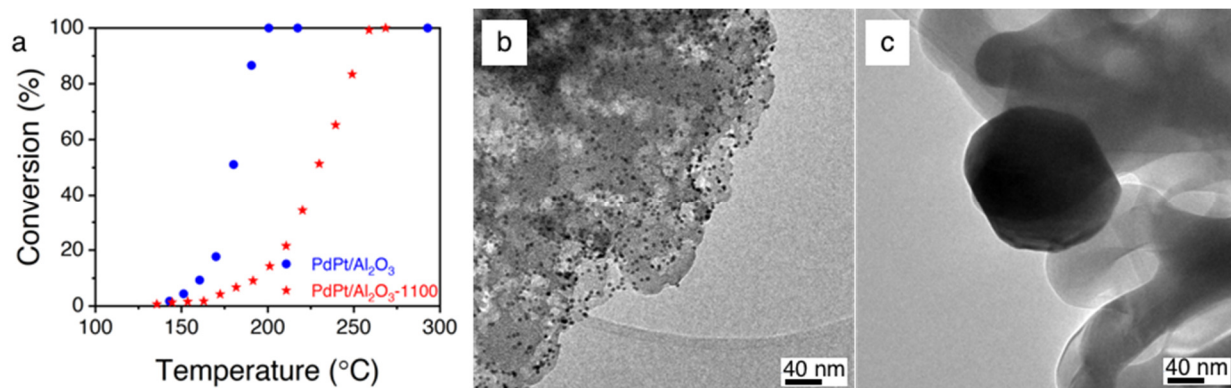
Figure S24. a) Propene combustion activity for fresh PdPt/Al$_2$O$_3$ and aged PdPt/Al$_2$O$_3$-1100. PdPt@Al$_2$O$_3$-1100 is the fresh catalyst aged at at 1,100 °C for for 5 h in air with 10 vol.% steam (40 ml/min total flow). Reaction mixture: 0.15 vol.% C$_3$H$_6$, 3 vol.% O$_2$, and 5 vol.% steam, balance Ar; b-c) Representative TEM images of fresh (b) and 1100°C aged (c) PdPt/Al$_2$O$_3$.
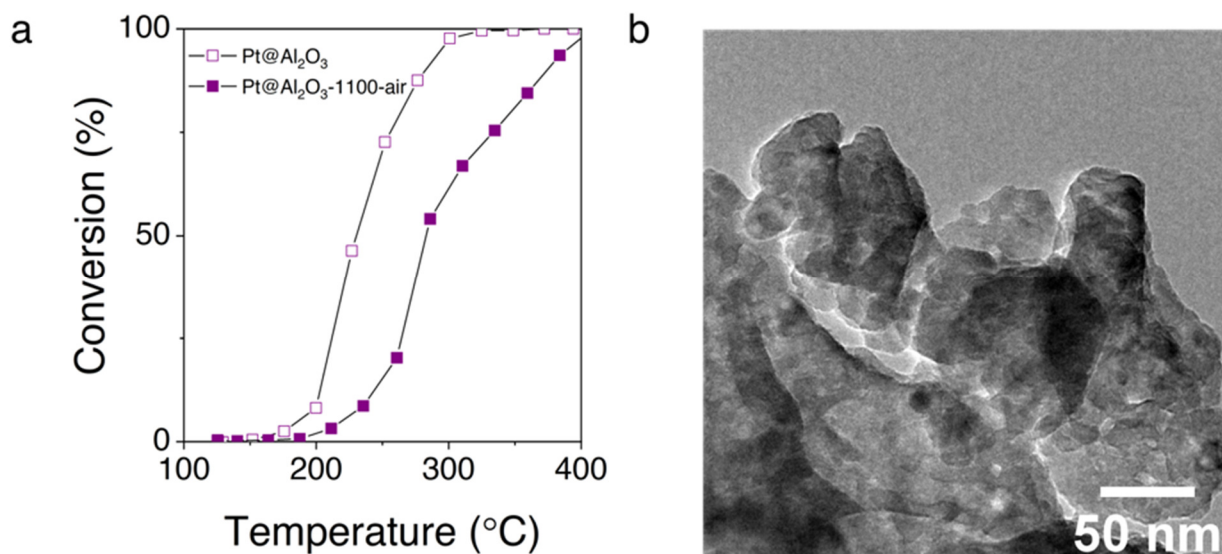
Figure S25. A) Propene combustion activity for fresh Pt@Al_2O_3 and 1,100 °C aged Pt@Al_2O_3. Reaction mixture: 0.15 vol.% C_3H_6, 3 vol.% O_2, and 5 vol.% steam. Aging performed at 1,100 °C for 5 h in air with 10 vol. % steam (40 ml/min total flow); b) TEM image of the 1,100 °C aged Pt@Al_2O_3 catalyst.

Figure S26. a) TEM image and particle size distribution of as-synthesized Pd@Al$_2$O$_3$; b) Propene combustion activity for fresh Pd@Al$_2$O$_3$ and 1,100 °C aged Pd@Al$_2$O$_3$. Reaction mixture: 0.15 vol.% C$_3$H$_6$, 3 vol.% O$_2$, and 5 vol.% steam. Aging performed at 1,100 °C for 5 h in air with 10 vol. % steam (40 ml/min total flow); c) TEM image of the 1,100 °C aged Pd@Al$_2$O$_3$ catalyst.
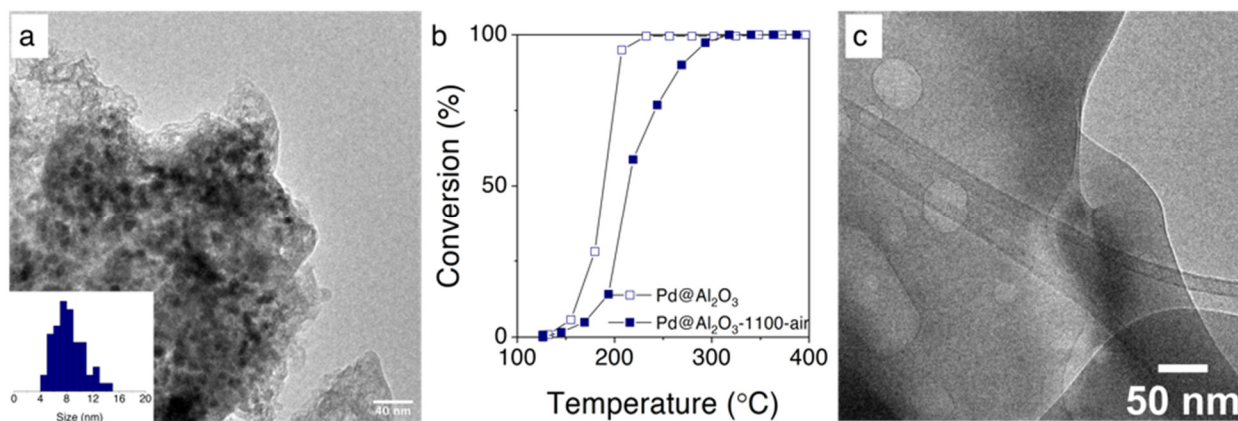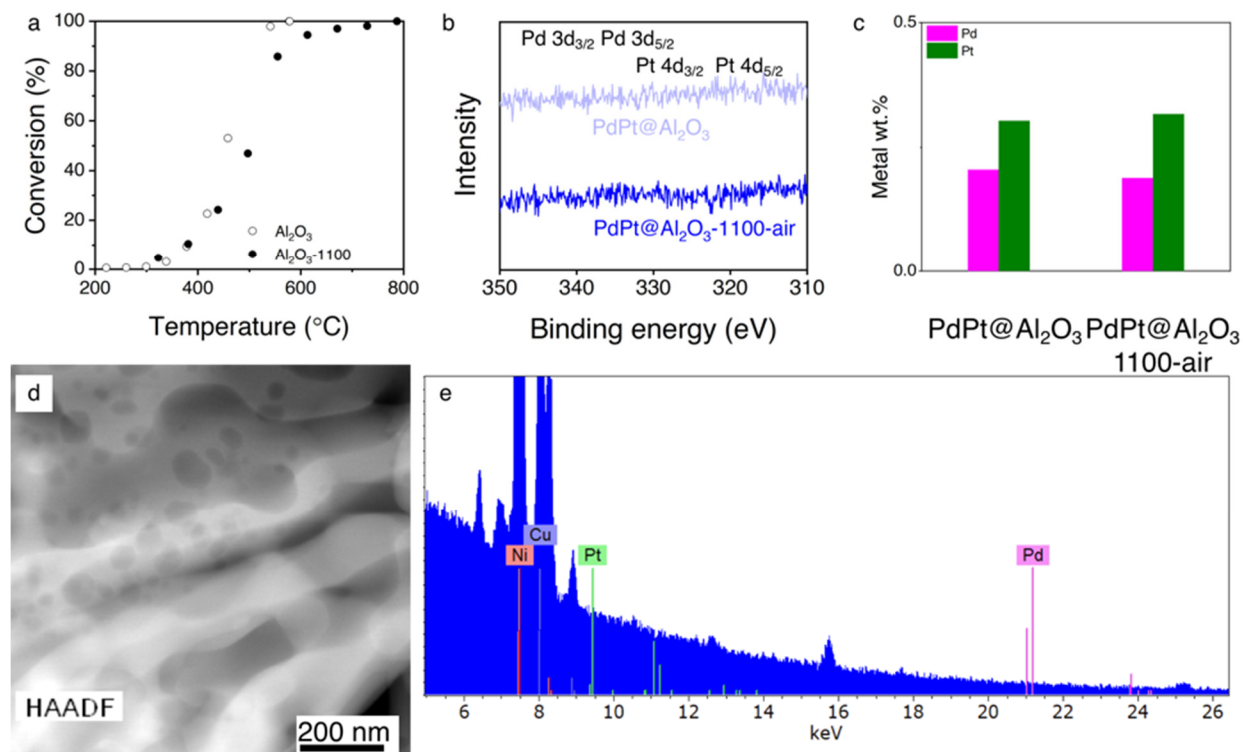
Figure S27. a) Propene combustion activity of the fresh and 1,100 °C aged metal-free alumina support. Reaction mixture: 0.15 vol.% C_3H_6, 3 vol.% O_2, and 5 vol.% steam. Aging performed at 1,100 °C for 5 h in air with 10 vol. % steam (40 ml/min total flow); b-c) Characterization of the as-synthesized and 1,100 °C aged PdPt@Al$_2$O$_3$: b) XPS; c) XRF; d-e) Representative HAADF-STEM image of 1,100 °C aged PdPt@Al$_2$O$_3$ and EDS spectrum showing no Pd or Pt detectable signal. Fe, Co, Cu, Zr and Sn normal signal from the TEM column/holder.
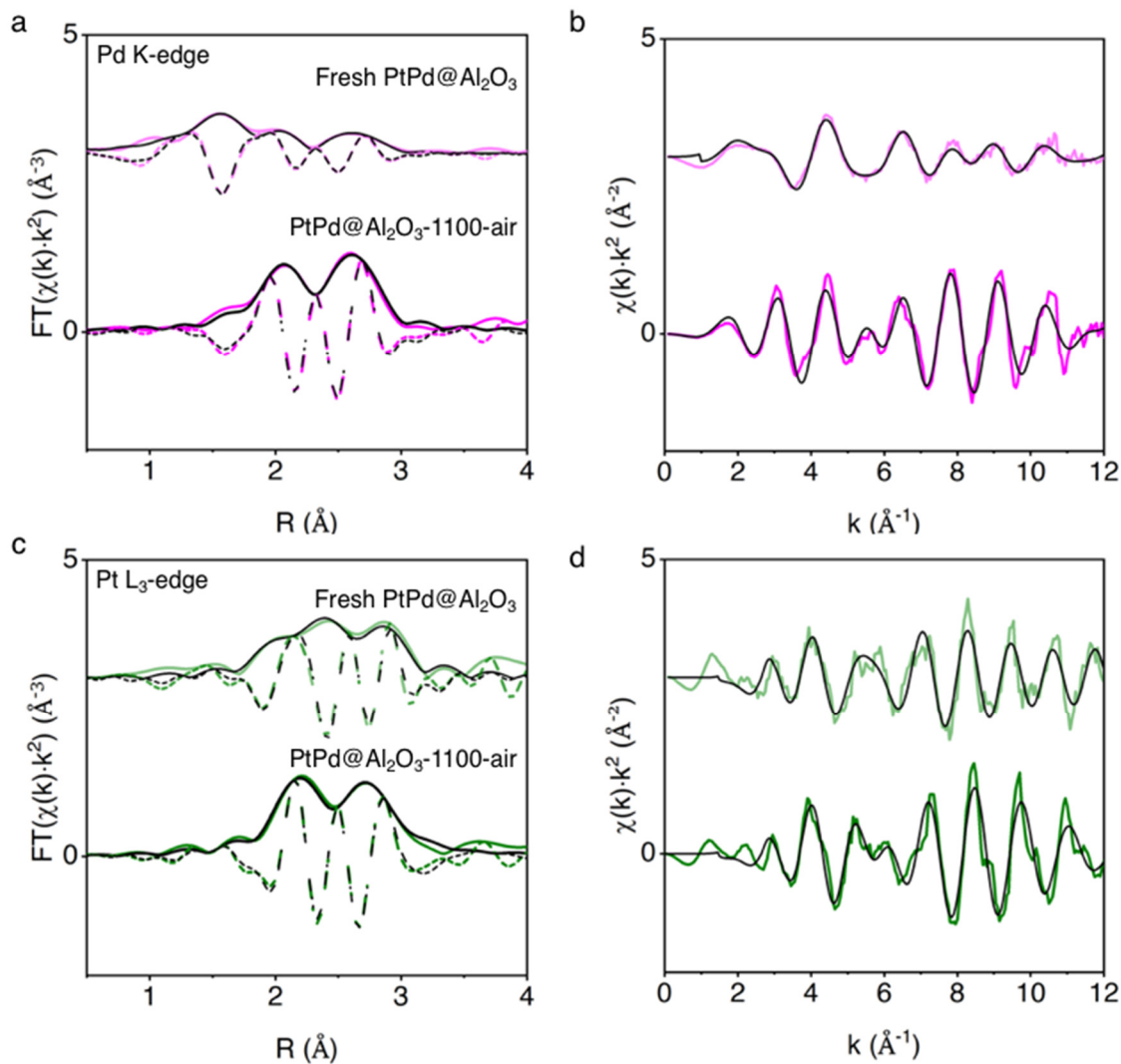
Figure S28. Magnitude and imaginary component of the Fourier Transform and EXAFS at the Pd K-edge (a-b) and Pt L₃-edge (c-d) characterizing the fresh PdPt@Al$_2$O$_3$ and PdPt@Al$_2$O$_3$-1100-air samples. Black lines indicate the fits. The range in R was 1.2-3.0 Å (Pd) and 1.7-3.2 Å (Pt); the range in k was 2.7-12.5 Å^{-1} (Pd) and 3.1-12.0 Å^{-1} (Pt).
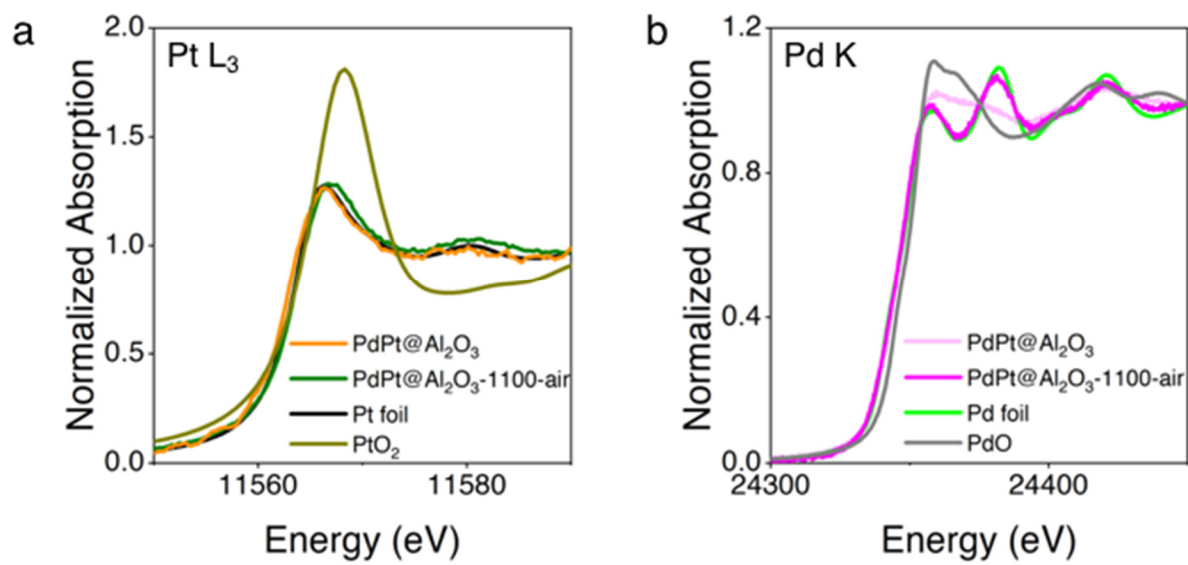
Figure S29. PdPt@Al$_2$O$_3$ XANES: a) Pt L$_3$-edge; b) Pd K-edge.
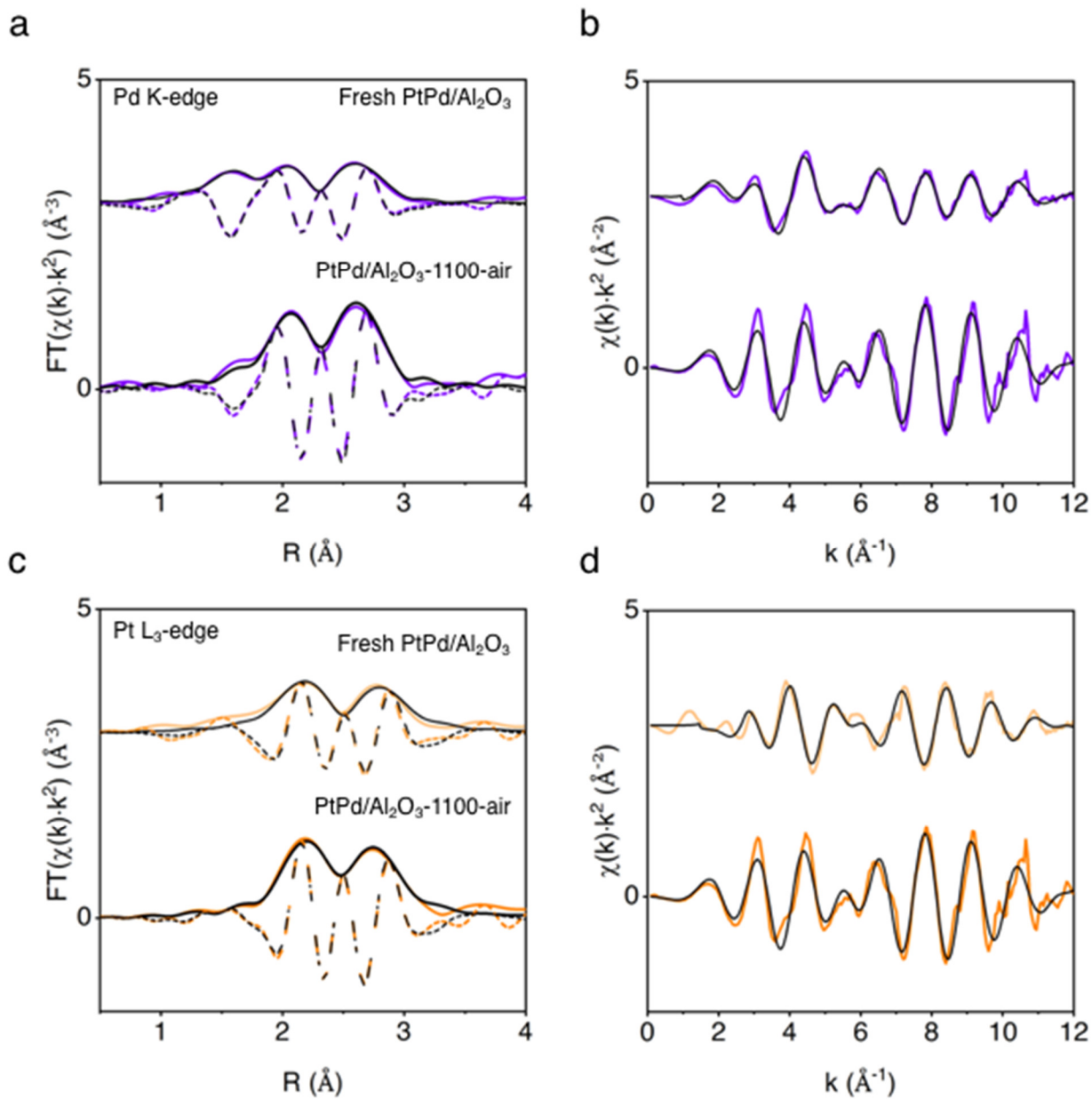
Figure S30. Magnitude and imaginary component of the Fourier Transform and EXAFS at the Pd K-edge (a-b) and Pt L$_3$-edge (c-d) characterizing the fresh PdPt/Al$_2$O$_3$ and PdPt/Al$_2$O$_3$-1100-air samples. Black lines indicate the fits. The range in R was 1.2-3.0 Å (Pd) and 1.7-3.2 Å (Pt); the range in k was 2.7-12.5 Å^{-1} (Pd) and 3.1-12.0 Å^{-1} (Pt).
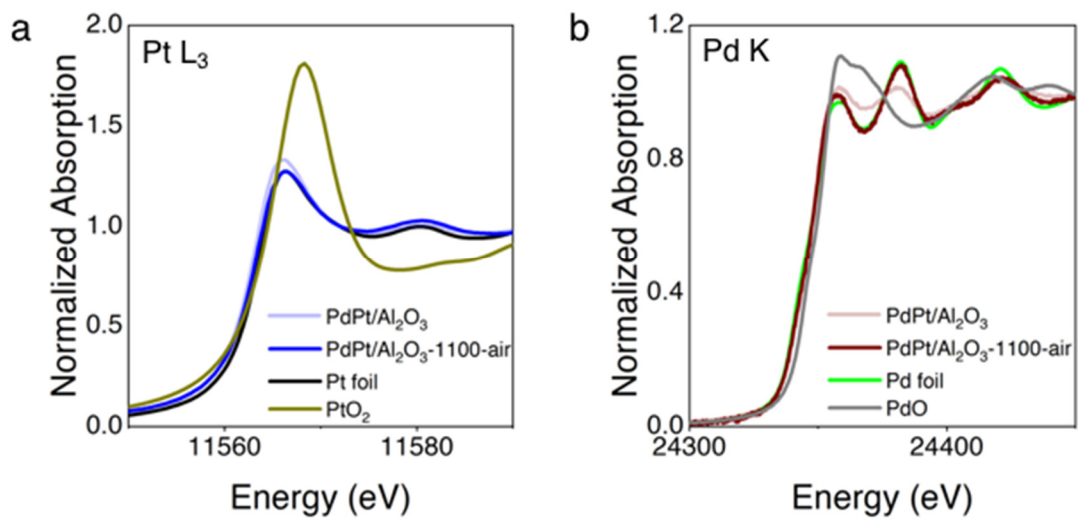
Figure S31. PdPt/Al$_2$O$_3$ XANES: a) Pt L$_3$-edge; b) Pd K-edge.
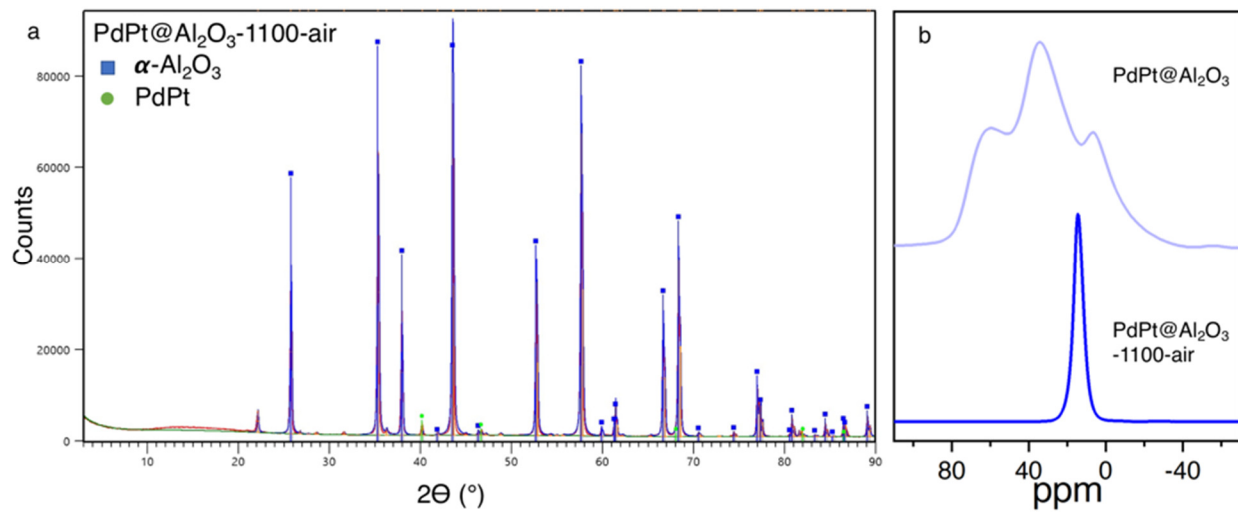
Figure S32. XRD (a) and ^{27}Al NMR (b) characterization of as-synthesized and 1,100 °C aged PdPt@Al$_2$O$_3$.
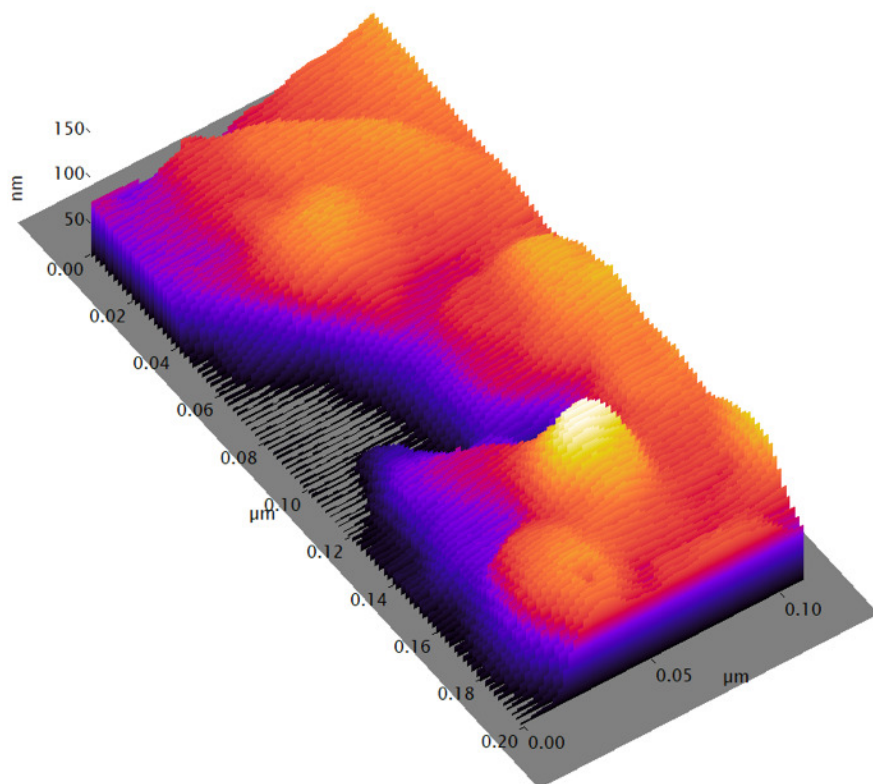
Figure S33. Thickness map of the supporting alumina layer in the as-prepared PdPt@Al$_2$O$_3$ sample crystallized into the α phase as determined from the log-ratio method of the low-loss portion of the EEL spectrum. Dimensions of the 3D surface plot are 200 nm x 110 nm x 167 nm (L x W x H).
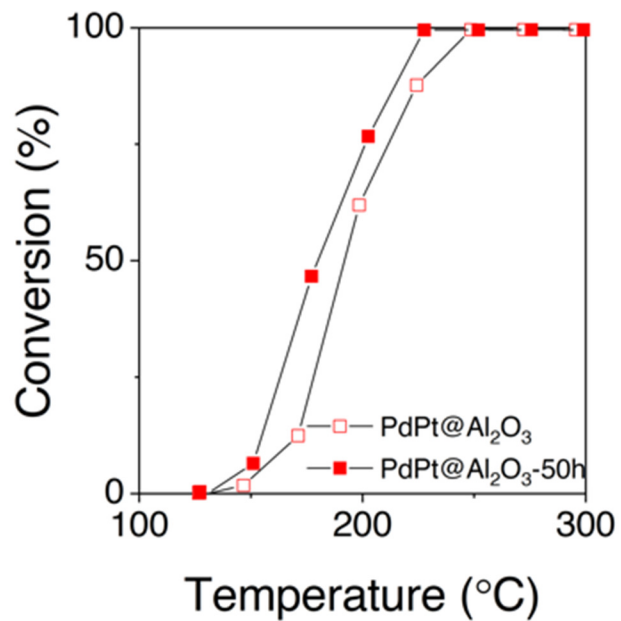
Figure S34. Propene combustion activity for fresh and aged PdPt@Al$_2$O$_3$. Aging performed for 50 h at 900 °C under alternating reducing-oxidizing conditions described in Table S5.
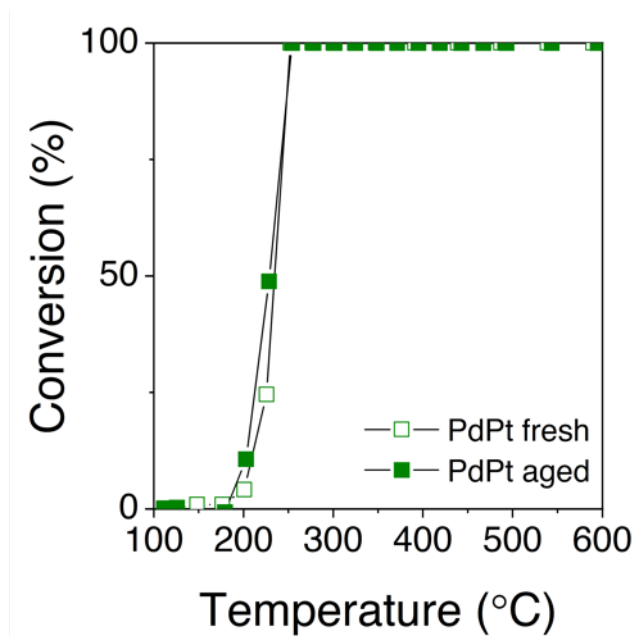
Figure S35. Propene combustion activity for fresh and aged PdPt@Al_2O_3. Aging performed for 48 h at 800 °C in the reaction mixture consisting of 2 vol. % CO_2, 0.2 vol. % CO, 0.1 vol. % C_3H_6, 0.1 vol. % C_3H_8, 5 vol. % H_2O, 8 vol. % O_2 balance Ar and N_2 (113 ml/min total flow). Catalyst mass: 31 mg. GHSV = 113,000 h^{-1}.
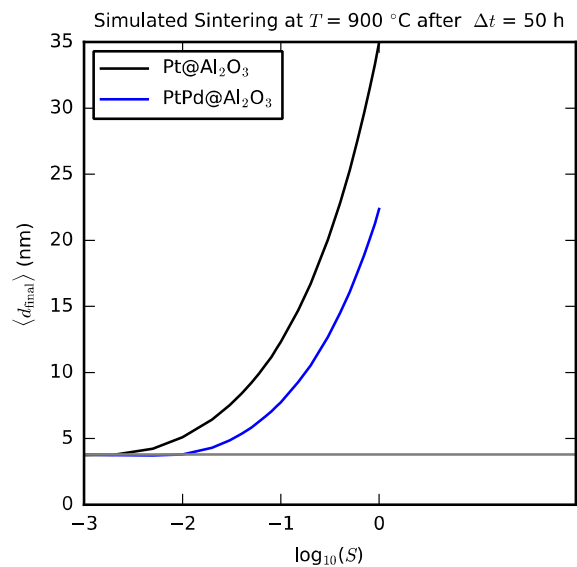
Figure S36. Sintering simulations at T = 900 °C for Pt@Al_2O_3 and PdPt@Al_2O_3 catalysts under 50 h of aging according to protocol reported in Table S5. The initial particle size distribution identical to that in Figure 3b. Since only sintering via PtO_2(g) is considered, the effective sintering time is 50/3 h ≈ 16.67 h (see further details for this protocol in Table S5). The effect of alloying with Pd is accounted for as a reduction of the surface energy by 21%.

Table S1. Platinum-alumina catalysts used in the study.

Catalyst	Description	Metal	Alumina support	Pt wt. % (XRF)
Pt@Al$_2$O$_3$	Pt NPs inside Al$_2$O$_3$		From polymer	0.44
Pt/Al$_2$O$_3$	Pt NPs on Al$_2$O$_3$	Colloidal Pt NPs from the same batch	From polymer	0.54
Pt/γ-Al$_2$O$_3$	Pt NPs on γ-Al$_2$O$_3$		Commercial γ-Al$_2$O$_3$	0.50
Pt-free Al$_2$O$_3$	Metal-free Al$_2$O$_3$	-	From polymer	-

Table S2. EXAFS fitting of Pt foil.

Sample	S_0^2	ΔE_0, eV	R, Å	σ^2, Å^2	CN$_{Pt\text{-}Pt}$
Pt foil	0.79 ± 0.06	9.8 ± 0.5	2.77 ± 0.01	0.005 ± 0.003	12

Table S3. Pt dispersion from CO chemisorption.

Sample	Pt@Al$_2$O$_3$	Pt@Al$_2$O$_3$-800	Pt/Al$_2$O$_3$	Pt/Al$_2$O$_3$-800
Pt dispersion, %	8.0	7.5	9.0	0.3

Table S4. PdPt- and Pd-alumina catalysts used in the study.

Catalyst	Description	Metal	Alumina support	Metal wt. % by XRF
PdPt@Al_2O_3	PdPt NPs inside Al_2O_3			0.51
Pd@Al_2O_3	Pd NPs inside Al_2O_3	Colloidal PdPt NPs	From polymer	0.4
PdPt/Al_2O_3	PdPt NPs on Al_2O_3			0.53

Table S5. Aging conditions of PdPt-, Pt-, and Pd-alumina catalysts.

Temperature, °C	O_2, vol.%	steam, vol.%	C_3H_6, vol.%	CO_2, vol.%	CO, vol.%	H_2, vol.%	C_3H_8, vol.%	Time, h	Catalyst
800	3	5	0.15	-	-	-	-	2	Pt@Al_2O_3 Pt/Al_2O_3 PdPt@Al_2O_3
800	3	10	-	-	-	-	-	2	Pt@Al_2O_3
800	3	5	0.15	-	-	-	-	2	Pt@Al_2O_3
1,100	21	10	-	-	-	-	-	5	Pt@Al_2O_3 Pd@Al_2O_3 PdPt@Al_2O_3
900	-/-/1.5	10/10/10	-	3/3/3	0/0.9/0	0/0.3/0	-	50	PdPt@Al_2O_3
800	8	5	0.1	2	0.2	-	0.1	48	PdPt@Al_2O_3

Table S6. EXAFS results for the fresh (as-synthesized) PdPt@Al_2O_3.

Edge	Scattering path	Fresh			
		CN	σ^2, Å^2	R, Å	ΔE_0, eV
Pd	Pd-O	2.1 ± 0.3	0.004 ± 0.001	2.03 ± 0.01	3.7 ± 1.1
	Pd-Pt	2.5 ± 0.6	0.006 ± 0.001	2.74 ± 0.03	-1.9 ± 0.6
	Pd-Pd	1.5 ± 0.3	0.005 ± 0.001	2.74 ± 0.03	-1.9 ± 0.6
Pt	Pt-Pt	10.5 ± 1.7	0.006 ± 0.001	2.74 ± 0.03	8.0 ± 0.6
	Pt-Pd	1.0 ± 0.8	0.006 ± 0.001	2.74 ± 0.03	8.0 ± 0.6

σ^2, mean-square deviation in path length; CN, coordination number; ΔE_0, inner potential correction. $S_0^2 = 0.78$ and 0.81 was used for Pd K-edge and Pt L_3-edge, respectively.

Table S7. EXAFS results for the 1,100 °C aged PdPt@Al_2O_3.

Edge	Scattering path	CN	σ^2, Å^2	R, Å	ΔE_0, eV
		1,100 °C aged			
Pd	Pd-O	-	-	-	-
	Pd-Pt	6.1 ± 0.5	0.003 ± 0.001	2.74 ± 0.04	-2.0 ± 0.3
	Pd-Pd	4.6 ± 0.4	0.003 ± 0.001	2.74 ± 0.04	-2.0 ± 0.3
Pt	Pt-Pt	5.4 ± 0.7	0.003 ± 0.001	2.74 ± 0.04	8.3 ± 0.5
	Pt-Pd	4.9 ± 0.4	0.003 ± 0.001	2.74 ± 0.04	8.3 ± 0.5

Table S8. EXAFS results for the fresh (as-synthesized) PdPt/Al$_2$O$_3$.

Edge	Scattering path	Fresh			
		CN	σ^2, Å^2	R, Å	ΔE_0, eV
Pd	Pd-O	1.4 ± 0.2	0.004 ± 0.001	2.03 ± 0.01	3.7 ± 1.1
	Pd-Pt	4.0 ± 0.5	0.006 ± 0.001	2.74 ± 0.03	-1.9 ± 0.6
	Pd-Pd	3.0 ± 0.4	0.005 ± 0.001	2.74 ± 0.03	-1.9 ± 0.6
Pt	Pt-Pt	6.3 ± 0.8	0.006 ± 0.001	2.74 ± 0.03	8.0 ± 0.6
	Pt-Pd	1.3 ± 0.5	0.006 ± 0.001	2.74 ± 0.03	8.0 ± 0.6

Table S9. EXAFS results for the 1,100 °C aged PdPt/Al$_2$O$_3$.

Edge	Scattering path	Fresh			
		CN	σ^2, Å^2	R, Å	ΔE_0, eV
Pd	Pd-O	-	-	-	-
	Pd-Pt	6.5 ± 0.6	0.003 ± 0.001	2.74 ± 0.04	-2.0 ± 0.3
	Pd-Pd	5.0 ± 0.5	0.003 ± 0.001	2.74 ± 0.04	-2.0 ± 0.3
Pt	Pt-Pt	5.8 ± 0.7	0.003 ± 0.001	2.74 ± 0.04	8.3 ± 0.5
	Pt-Pd	4.4 ± 0.4	0.003 ± 0.001	2.74 ± 0.04	8.3 ± 0.5

References

1   Wynblatt, P. & Gjostein, N. A. Particle growth in model supported metal catalysts—I. Theory. *Acta Metall.* **24**, 1165-1174 (1976).